J Comput Neurosci
DOI 10.1007/s10827-008-0076-8

On the derivation and tuning of phase oscillator models for lamprey central pattern generators

Péter L. Várkonyi · Tim Kiemel · Kathleen Hoffman · Avis H. Cohen · Philip Holmes

Received: 31 August 2007 / Revised: 10 December 2007 / Accepted: 16 January 2008

Abstract Using phase response curves and averaging theory, we derive phase oscillator models for the lamprey central pattern generator from two biophysically-based segmental models. The first one relies on network dynamics within a segment to produce the rhythm, while the second contains bursting cells. We study intersegmental coordination and show that the former class of models shows more robust behavior over the animal's range of swimming frequencies. The network-based model can also easily produce approximately constant phase lags along the spinal cord, as observed experimentally. Precise control of phase lags in the network-based model is obtained by varying the relative strengths of its six different connection types with distance in a phase model with separate coupling functions for each connection type. The phase model also describes the effect of randomized connections, accurately predicting how quickly random network-based models approach the determinisitic model as the number of connections increases.

Keywords Phase reduction · Lamprey · Intersegmental coordination · Bursting · Network effect

Action Editor: Karen Sigvardt

P. L. Várkonyi (✉)
Department of Mechanics, Materials and Structures, Budapest University of Technology and Economics, Muegyetem rkp. 1-3, 1111 Budapest, Hungary
e-mail: vpeter@mit.bme.hu

T. Kiemel
Department of Kinesiology, University of Maryland, College Park, College Park, MD 20742, USA

K. Hoffman
Department of Mathematics and Statistics, University of Maryland, Baltimore County, Baltimore, MD 21250, USA

A. H. Cohen
Department of Biology and Institute for Systems Research, University of Maryland, College Park, College Park, MD 20742, USA

P. Holmes
Program in Applied and Computational Mathematics and Department of Mechanical and Aerospace Engineering, Princeton University, Princeton, NJ 08544, USA

1 Introduction

Central pattern generators (CPGs) are neural networks that can produce functional patterns of muscular activity in the absence of sensory feedback [see e.g. Getting 1988; Cohen et al. 1988; Pearson 2000 and Wilson 1999, Chaps. 12-13] or other inputs such as those from the brain. Across a wide variety of animals, from invertebrates to mammals, the CPGs that underlie locomotion have been found to be distributed systems of non-linear oscillators coupled through ascending and descending neurons. In leech (Kristan et al. 2005), lamprey (Grillner 2003), and neonatal rats (Kiehn 2006), the oscillators are themselves composed of networks of neurons with connections that produce alternation among antagonistic muscles either across joints or segments. In addition, many of the network neurons have complex membrane properties that, when activated, confer the ability to oscillate independently.

This paper describes a framework for modeling distributed CPGs. Focusing on the locomotory system of

lamprey, we examine two generic forms of CPG model: one network-based and the other cell-based. In the former, the pattern emerges from connections among the neurons, while in the latter it is due to intrinsic properties of single neurons or of a small group of oscillatory neurons.

The lamprey CPG for locomotion itself consists of interneurons and motoneurons distributed along the spinal cord. Suitably stimulated, an isolated spinal cord *in vitro*, with brain, muscle, and afferent inputs removed, exhibits fictive locomotion, producing approximately periodic bursts of action potentials from motoneurons via the ventral roots (Cohen and Wallén 1980). Contralateral roots burst in antiphase, and ipsilateral roots along the spinal cord exhibit a phase lag of $1-2\%$ of the bursting period, leading to propagation of a traveling wave comprising approximately one full wavelength along the ≈ 100-segment cord (Williams and Wallén 1984). Sections containing as few as four segments can produce bursts, suggesting that the CPG is a chain of localized oscillatory units. Furthermore, each side of the spinal cord is capable of generating oscillations (Cangiano and Grillner 2003). For further background information, see Cohen et al. (1992) and Grillner (2003).

There is no complete agreement as to the composition of the lamprey CPG. Several different cell types, common to each segment, have been identified and their interconnections, both within and among segments, have been partially described (Rovainen 1974; Buchanan 1982; Buchanan and Grillner 1987; Buchanan 2001), as have membrane properties capable of generating intrinsic oscillations within a hemisegment (Schotland and Grillner 1993; Kotaleski et al. 1999b; Cangiano and Grillner 2003). Models involving three of these neuronal classes have been proposed, but it is known that other neurons very probably contribute to the network (Parker 2006). Similarly, the critical intrinsic properties remain to be identified, with some incorporated into models, and others to be omitted. Evidence on the exact nature of intersegmental coordinating neurons is very incomplete, but it is clear that connections are ascending, descending, long and short, and overall quite strong (Rovainen 1985; Miller and Sigvardt 2000; Kiemel et al. 2003).

In the absence of detailed architectural information, some early models of lamprey CPG were phenomenological: single chains of phase oscillators of the form

$$\dot{\phi}_i = \omega_i + h_i(\phi_1, \phi_2, \ldots, \phi_n)\,, \quad i = 1, 2, \ldots, n\,, \tag{1}$$

where ϕ_i denotes the phase of the ith unit in the chain and the coupling functions h_i are 2π-periodic in each of the phases. These models produce ipsilateral phase lags either by frequency gradients $\omega_i > \omega_{i+1}$ (Cohen et al. 1982), or by asymmetrical coupling in the rostral and caudal directions (Ermentrout and Kopell 1984, 1991; Kopell and Ermentrout 1988). Simple sinusoidal coupling functions $h_i = \alpha_{ji} \sin(\phi_j - \phi_i)$ were typically assumed, as in the Kuramoto rotator model (Kuramoto 1984). Whatever proves to be the correct structure, there is clear evidence that the spinal segments comprise a chain of oscillators coupled together to produce a traveling wave motion in the body.

In this paper we review and compare two segmental models that share the same network architecture (Buchanan and Grillner 1987) but are based on the different rhythm-generating mechanisms noted in (Grillner et al. 1988). Our *cell-based* model, inspired by Grillner et al. (Wallen et al. 1992; Hellgren et al. 1992), contains spontaneously bursting neurons within each hemisegment, while the *network-based* scheme of Buchanan and Williams (Buchanan 1992; Williams 1992), relies on contralateral mutual inhibition in the manner of a half-center oscillator. Both have stable limit cycles and we use phase reduction and averaging (Hoppensteadt and Izhikevich 1997) to compute intersegmental coupling functions h_i, extending the study of Williams and Bowtell (1997), who found such functions for the network-based model with nearest-neighbor coupling. (For the cell-based model we also find intrasegmental coupling functions.) This adds biological detail to the simple models of (Cohen et al. 1982; Ermentrout and Kopell 1984; Kopell and Ermentrout 1988) and allows us to study the robustness of phase lags and the traveling wave pattern as the overall level of excitation, and hence swimming speed, changes.

Current network-based models employ population (firing-rate) descriptions, while cell-based oscillators have mostly used bursting cell descriptions (see however Ekeberg 1993; Wilson 1999). Phase response and averaging techniques can be applied to models of both types (for recent examples with bursting cells, see (Ghigliazza and Holmes 2004a, b), but to more directly compare the two mechanisms, here we treat only population models. As noted in Section 4.2, the behavior of our averaged population model agrees well with numerical simulations of bursters, despite multiple simplifications in its derivation. Our goal is twofold: to justify phase oscillators as models for lamprey CPG, showing that they can include and allow comparison of biophysical details, and to investigate and compare how cell type and coupling details contribute to the traveling waves characteristic of fictive swimming in lamprey.

In Section 2 we outline the use of the phase reduction and averaging theory that is used in Sections 3–5 to compute phase response curves (PRCs) and coupling

functions for the cell- and network-based models. Section 3 concerns the reduction of intrasegmental models to phase oscillators, and Section 4 deals with coupling along the cord. Section 5 describes a tuning mechanism for each type of connection and in Section 5.2 the connections from the tuned deterministic model in the previous section are randomized. The paper concludes in Section 6.

2 Phase reduction and averaging

Here we briefly review the tools to be used in this paper. Phase reduction theory was originally developed by Malkin (1949, 1956) and is discussed in (Ermentrout and Kopell 1991; Ermentrout 1996; Hoppensteadt and Izhikevich 1997). It allows one to describe interactions among weakly-coupled oscillators of the form

$$\dot{\mathbf{x}}_i = \mathbf{f}(\mathbf{x}_i) + \epsilon \mathbf{g}(\mathbf{x}_i, \mathbf{x}_j, \ldots)\,;\ \mathbf{x}_i = \left(x_i^1, \ldots, x_i^n\right) \in \mathbb{R}^n\,,$$
$$\epsilon \ll 1\,, \tag{2}$$

each possessing a hyperbolic limit cycle Γ_i of period $T_0 = 2\pi/\omega_0$, solely in terms of their phases along Γ_i:

$$\dot{\phi}_i = \omega_0 + \epsilon \mathbf{z}(\phi_i) \cdot \mathbf{g}(\mathbf{x}_i(\phi_i), \mathbf{x}_i(\phi_j), \ldots)\,|_{\Gamma_0(\phi_i)} + \mathcal{O}(\epsilon^2)\,. \tag{3}$$

In (3) the vector-valued function $\mathbf{z}(\phi_i) \stackrel{\text{def}}{=} \frac{\partial \phi_i}{\partial \mathbf{x}_i}$ encodes the asymptotic phase shifts due to infinitesimal impulsive perturbations in the directions x_i^k; each component of $\mathbf{z}(\phi_i)$ is called a PRC. PRCs may be computed via an adjoint method or directly, by perturbative or numerical means, as will be done below.

Substituting the slow phase $\psi_i = \phi_i - \omega_0 t$ into (3) removes the fast frequency ω_0, so that the averaging theorem (Guckenheimer and Holmes 1983, Sections 4.1–2) can be applied to yield ordinary differential equations (ODEs) that depend, at leading order, only on phase differences:

$$\dot{\psi}_i = \epsilon \bar{H}_i(\psi_i - \psi_j) + \mathcal{O}(\epsilon^2) \text{where} \tag{4}$$

$$\bar{H}_i(\psi_i - \psi_j) = \frac{1}{T_0} \int_0^{T_0} \mathbf{z}(\phi_i) \cdot \mathbf{g}(\mathbf{x}_i(\psi_i + \omega_0 t),\ \mathbf{x}_i(\psi_j + \omega_0 t), \ldots)\, dt\,. \tag{5}$$

If the coupling function $\mathbf{g}$ of Eqs. (2–3) is additive, as in Sections 3–5, (5) implies that the effects of multiple connections into a given unit are approximated by linear superposition.

To further prepare for the analyses below, we consider a pair of symmetrically coupled units, in which case the coupling functions share a common form $\bar{H}$. The averaged equations (4) can then be subtracted to yield a single ODE for the phase difference $\psi_{ij} \stackrel{\text{def}}{=} \psi_i - \psi_j = \phi_i - \phi_j$:

$$\dot{\psi}_{ij} = \epsilon[\bar{H}(\psi_{ij}) - \bar{H}(-\psi_{ij})] \stackrel{\text{def}}{=} \epsilon G(\psi_{ij})\,, \tag{6}$$

where we neglect terms of $\mathcal{O}(\epsilon^2)$. Since $\bar{H}$ is 2π-periodic, $G(\pi) = \bar{H}(\pi) - \bar{H}(-\pi) = \bar{H}(\pi) - \bar{H}(\pi) = 0$ and $G(0) = \bar{H}(0) - \bar{H}(0) = 0$, implying that fixed points corresponding to in-phase and anti-phase solutions *always* exist, regardless of the form of $\bar{H}$. Fixed points $\psi^* \neq 0, \pi$ may also exist, and they and the stability properties of all fixed points depend on the details of $\bar{H}$.

3 Phase reduction of segmental CPG models

As noted in the introduction, the lamprey CPG is generally modeled as a chain of coupled units, each of which can produce periodic bursts in isolation. As we have noted, a functional unit may not coincide with a single segment of the spinal cord, but we shall loosely identify units with segments.

The intrasegmental architecture of Fig. 1 was proposed in Buchanan and Grillner (1987), and slightly different versions of this network have been used elsewhere. There is now evidence that more neurons participate in the basic unit (Parker 2006), but Fig. 1 is a good place-holder for the detailed network. In this model, inhibitory connections between the two sides are considered important for the oscillations. Initial experiments to determine whether isolated hemisegments can oscillate produced inconclusive results (e.g. Harris-Warrick and Cohen 1985; Buchanan 1999). However, more recent results provide much greater support

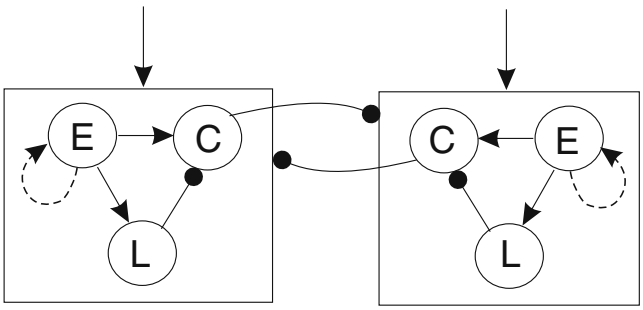

Fig. 1 The structure of the segmental oscillator proposed in (Buchanan and Grillner 1987). *E*, *C* and *L* denote excitatory, crossed inhibitory, and lateral inhibitory cells respectively. *Arrows* and *filled circles* denote excitatory and inhibitory connections respectively. C cells inhibit all units on the opposite side. E–E connections (*dashed arrows*) are excluded in some models. In this study, we compare cell-based models with E–E connections to network-based ones without them

Table 1 Parameters of the network-based model

Name	Meaning	Value in Sections 3-4	Value in Section 5
e_E	Tonic drive to E,L,C cells	$0.005 - 0.07$ except in Fig. 7(right)	$0.01 - 0.075$
e_L		0.01 except in Fig. 7(right)	0.01
e_C		0.1 except in Fig. 7(right)	0.1
τ_i	Time constant of dynamics	10	10
w_{ij}	Strength of intrasegmental connection from cell type i to j	1 for all i, j, except for the tuned model in Section 5	
A_a	Basic value of ascending/	Variable, see Section 4.1	0.02 or 0.4
A_d	descending intersegmental connection strength in chains	Variable, see Section 4.1	0.005 or 0.1
λ_a	Space constant for decay of ascending/descending interseg-	$\ln(2)^{-1} \approx 1.44$	Variable
λ_d	mental connection strength with distance in chains	$\ln(2)^{-1} \approx 1.44$	Variable
l_a	Maximal length of ascending/	5	10
l_d	descending intersegmental connections in chains	5	10

for the oscillatory capability of the hemi-segment (Cangiano and Grillner 2003). For purposes of the current analysis, we shall compare and analyze simplified models of both network-based segmental and cell-based hemisegmental oscillators, and explore their similarities and differences. In Section 4 we consider chains built of both types of units in order to study intersegmental coordination. We shall also discuss the limits of applicability of phase reduction methods.

3.1 A network-based segmental oscillator

Our network-based model is due to (Buchanan 1992; Williams 1992) and has the same architecture as that of (Buchanan and Grillner 1987). Six ODEs describe the two sets of three cell types. Each type is characterized by an activity variable $a = a(t)$, representing a population of cells with average firing rate $f(a)$:

$$f(a) = [a]_+ \stackrel{\text{def}}{=} \left\{ \begin{array}{l} f(a) = a \; if \; a \geq 0 \\ f(a) = 0 \; if \; a < 0 \end{array} \right\} , \tag{7}$$

and the dynamics of the i^{th} population is governed by the dimensionless equation

$$\dot{a}_i = e_i(v_{ie} - a_i) - \tau_i^{-1} a_i + \sum_j w_{ij} f(a_j)(v_{ij} - a_i) , \tag{8}$$

where e_i and v_{ie} are the strength and reversal potential of the tonic drive to population i, $f(a_j)$ is the firing rate of population j, and w_{ij} and v_{ij} are the strength and reversal potential of the coupling from j and i. As in (Williams 1992) the following parameters were used: $\tau_i = 10$, $v_{ie} = 1$, $v_{ij} = +1$ and -1 for excitatory and inhibitory connections respectively, and $w_{ij} = 1$ for all intrasegmental coupling strengths. Excitatory E-E feedback, shown dashed in Fig. 1, was not included. Tonic drives were $e_L = 0.01$, $e_C = 0.1$ for L and C cells, and were varied from $e_E = 0.005$ to 0.07 for E cells, allowing oscillation frequency to span a three-fold range. For reference, all parameter values for this and for the cell-based model are given in Tables 1 and 2.

As noted in Williams (1992), the essential units are L and C cells. Contralateral inhibitory connections from C cells ensure that one hemisegment is silent while the other is active, and L cells terminate the activity of ipsilateral C cells, resulting in antiphase left-right activity. As this suggests, on each side C cells activate first, followed by L and E cells, as illustrated in the upper panels of Fig. 2, and the hemisegments burst in antiphase as in fictive swimming (Buchanan 2001).

We computed PRCs via a numerical realization of the direct method (Hoppensteadt and Izhikevich 1997): see Fig. 2 (lower panels). Due to bilateral symmetry, PRCs are only shown for one hemisegment, although for this network-based oscillator, the limit cycle must be viewed in the full six-dimensional space. These PRCs will be used in Section 4 to determine coupling functions between segments along the chain.

3.2 A pair of cell-based segmental oscillators

Our cell-based model is inspired by the detailed biophysical models of (Wallen et al. 1992; Hellgren et al. 1992; Lansner 1997; Kotaleski et al. 1999b) and the simplified versions of (Ekeberg 1993; Wilson

Table 2 Parameters of the cell-based model

Name	Meaning	Value
e	Tonic drive to all cell types	$0.05 - 0.15$
w_{ij}	Strength of intrasegmental connection from cell type i to j	± 1 for all i, j
g	Parameters of the Naka-	1.2
s	Rushton function (11)	0.1

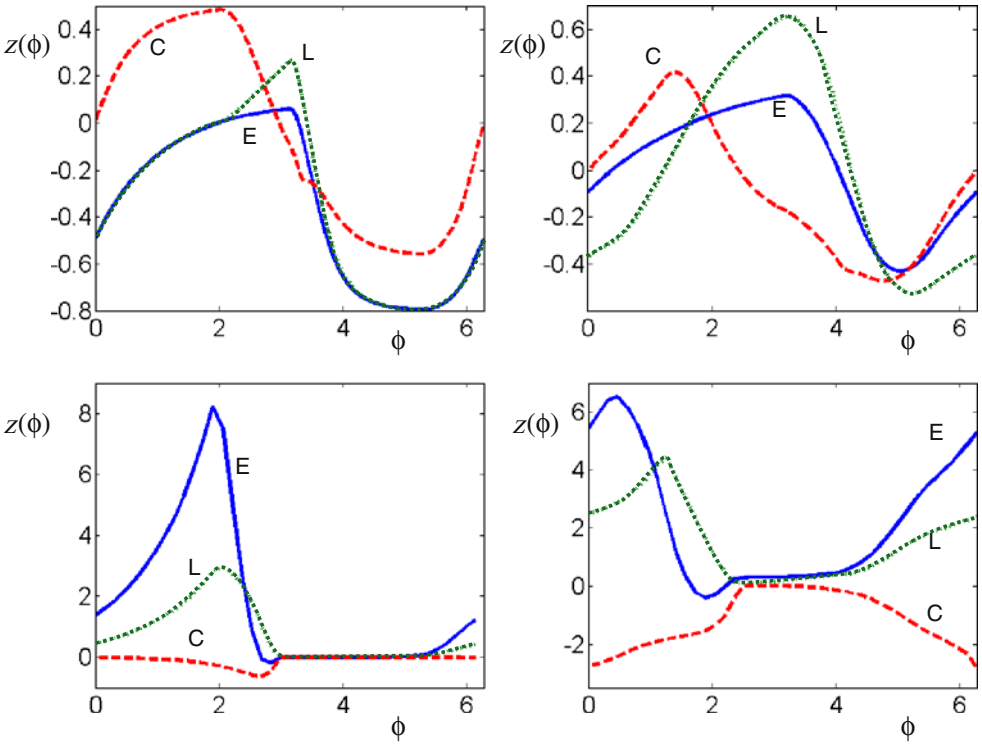

Fig. 2 Time series (*top*) and PRCs (*bottom*) for the network-based model of (Williams 1992) at $e_E = 0.01$ (*left*) and 0.07 (*right*). Outputs of E, L, and C cells in one hemisegment are shown *solid*, *dotted* and *dashed* respectively; those of the opposite hemisegment are identical in form but π out of phase

1999). In simulations reported in (Wallen et al. 1992; Hellgren et al. 1992; Lansner 1997; Kotaleski et al. 1999b) the units E,L and C of Fig. 1 are each represented by a multi-compartment Hodgkin-Huxley type neuron with 3 or 4 ion channels governed by 10-12 coupled ODEs (Wallen et al. 1992), or by a population of such cells (Hellgren et al. 1992). In these papers the role of slow after-hyperpolarizing (AHP) currents acting through Ca^{2+} dependent K^+ channels is emphasized. The E cells are assumed to be self-excitatory and parameters are chosen so that they exhibit bursts terminated by slow accumulation of the AHP current [although in some models contralateral inhibition is also required for burst termination (Kotaleski et al. 1999a)]. Thus, the core of these models is a group of bursting cells in each hemisegment with mutual inhibition causing alternating activity. Distinguishing between E and C cells is not essential, although it increases the stability of the oscillations (Hellgren et al. 1992), and L cells, which are of primary importance in the network-based model, play little role in the cell-based simulations. Indeed, in Lansner (1997) L cells were completely excluded from the network, thereby increasing its frequency range. However, see Parker (2006) for a critique of this reduction.

Bursting frequency in cell-based models can be changed by varying the tonic drive, presumably via a variety of mechanisms. For example, frequency would be increased by raising the concentration of glutamate either from descending inputs or other excitatory sources such as neuromodulatory inputs that prolong plateau potentials. Frequency would be decreased by increasing the serotonin concentration either from intrinsic serotonergic neurons or by descending or sensory serotonergic inputs (Schotland and Grillner 1993) (but also see Parker 2006). Other mechanisms will certainly be identified.

In place of such biophysically-detailed spiking models, here we introduce a minimal spike-rate model inspired by Ekeberg (1993) and Wilson (1999). Each unit is described by dimensionless activation and recovery variables a_i and r_i respectively, the latter accounting for spike rate adaptation due to AHP currents:

$$\dot{a}_i = -a_i + e + \sum_j w_{ij} N(a_j, r_j)\,, \tag{9}$$

$$\tau_i(e)\dot{r}_i = N(a_i, r_i) - r_i\,. \tag{10}$$

Here e is the common tonic drive to each cell and w_{ij} are signed coupling strengths, positive for excitatory and negative for inhibitory connections. In this model, firing rates are described by a Naka-Rushton function:

$$N(a_j, r_j) = \frac{[a_j - g r_j]_+^2}{s^2 + [a_j - g r_j]_+^2}\,, \tag{11}$$

which, unlike the piecewise-linear function of Eq. (7), sets an upper bound on neural activity. The parameters

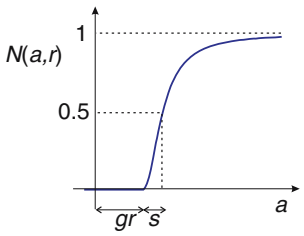

Fig. 3 The Naka-Rushton function $N(a, r)$: a represents excitation level of cells and r is the level of spike-rate adaptation due to slow AHP currents. Parameter values are $s = 0.1$, $g = 1.2$

g and s determine firing onset and the steepness with which it rises: see Fig. 3.

Serotonin modulation (Schotland and Grillner 1993) is included by allowing e to change the time scale of the recovery dynamics, as in Wilson (1999):

$$\tau_i(e) = \frac{40}{1 + (20e)^2}\,. \tag{12}$$

From (11), high values of r correspond to reduced excitability, and (10) implies that r_i slowly increases during bursting and decreases during silent periods for all cell types. However, the oscillatory properties are primarily determined by E cells; thus we first consider these alone. Limit cycles and PRCs for an isolated E cell are shown in Fig. 4. Within each hemisegment E, L, and C cells all share common tonic drive e and excitation from the E cells, and although C cells are additionally inhibited by L's, all cell types exhibit similar dynamics. Indeed, with appropriately balanced connection strengths, e.g. $w_{EE} = w_{EL} = 1$; $w_{LC} = -1$, $w_{EC} = 2$, the hemisegment exhibits *identical* dynamics in all three units (modulo transients due to initial conditions). Parameter values for the Naka-Rushton firing rate function were $s = 0.1$, $g = 1.2$, and the tonic drive e was varied from 0.05 to 0.15: see Table 2.

In this cell-based model, each hemisegment produces a limit cycle oscillation, and derivation of PRCs for a hemisegment is straightforward if those of individual E cells are known (Fig. 4). Since there is no feedback to E from L or C cells, perturbing the latter yields no net phase shift after transients have decayed: hence the PRCs for L and C cells are identically zero. This suggests that the hemisegmental network can be reduced by removing all external inputs to L and C cells (due to their zero PRCs), and reassigning their outgoing connections to the E cells (due to the identical dynamics), thereby effectively eliminating L and C cells. It also explains why L cells were found to have little role in simulations and have been eliminated in recent cell-based models (Kotaleski et al. 1999a).

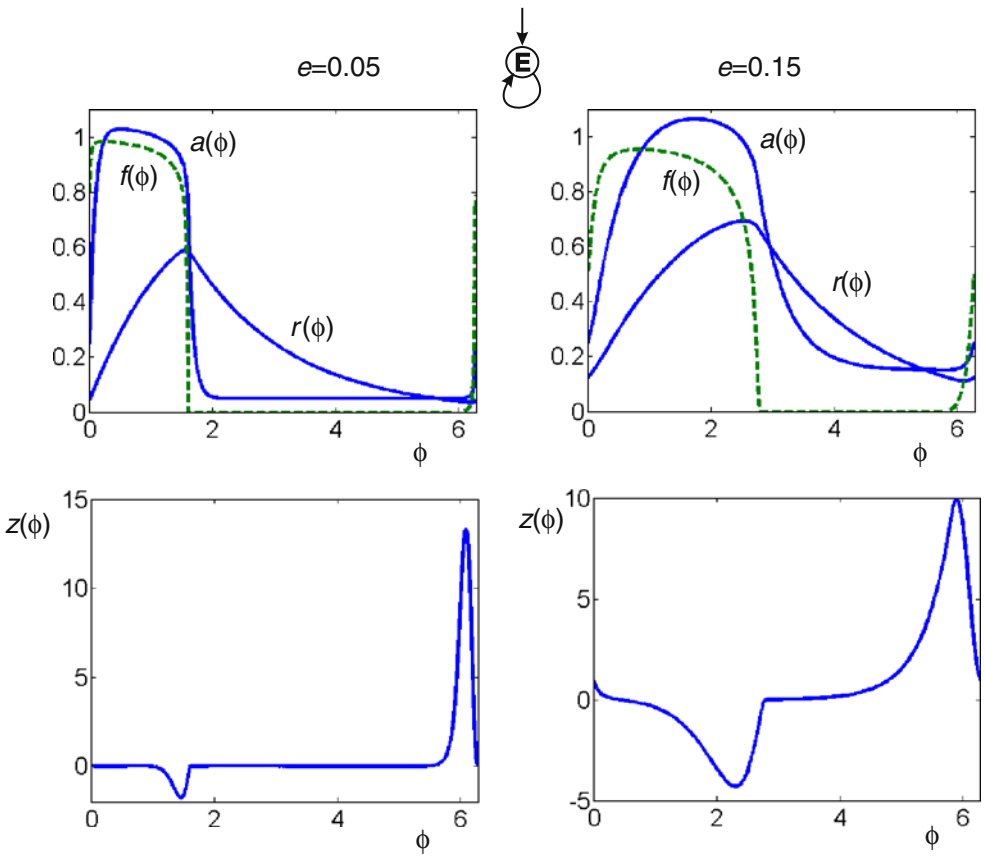

Fig. 4 Time series of activation and recovery variables and firing rate f (*top*), and PRCs (*bottom*) of bursting E cells with self-excitation in the reduced cell-based oscillator for input levels $e = 0.05$ (*left*) and $e = 0.15$ (*right*). Periods are $T = 74.03$ and $T = 17.26$ respectively

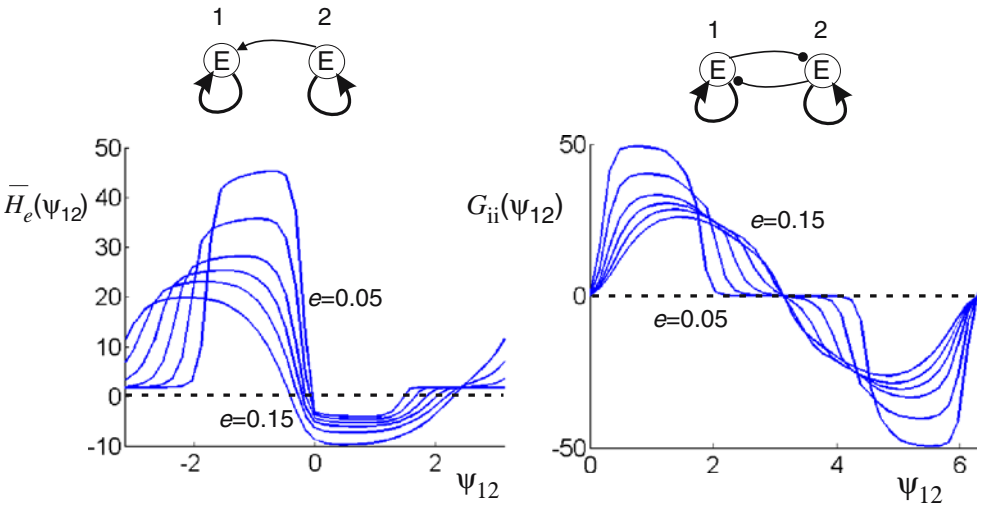

Fig. 5 The coupling function of a pair of reduced cell-based oscillators with unidirectional excitatory coupling ($\bar{H}_e$, *left panel*), and with symmetric mutual inhibition (G_{ii}, *right panel*). Roots of G_{ii} with negative derivatives correspond to stable phase-locked solutions. Here the antiphase solution ($\psi_{12} = \pi$) is the unique stable one

We shall use the reduced E cell hemisegment of Fig. 4 as a building block for the segmental CPG in Section 4.2, below. We prepare for this by examining the behavior of two coupled hemisegments, which is done in two steps. We first compute the averaged coupling function $\bar{H}_e(\psi_{12})$ of a hemisegment that receives weak excitation from a similar unit, obtaining the left panel of Fig. 5. This shows that $\bar{H}_e(\psi_{12})$ has a stable fixed point close to $\psi_{12} = 0$, implying that the driven cell 1 bursts almost in phase with the driver 2, with a phase lag that increases with tonic drive amplitude e.

In the weak coupling limit under phase reduction, inhibitory connections are obtained from excitatory ones by a simple change of sign. The averaged coupling function for symmetric inhibition is therefore

$$G_{ii}(\psi_{12}) = -\bar{H}_e(\psi_{12}) + \bar{H}_e(-\psi_{12}) \tag{13}$$

(cf. Eq. (6)). As noted in Section 2, there are fixed points at $\psi_{12} = 0$ and π, and the right panel of Fig. 5 reveals that the former is always unstable and the latter stable, but that its stability becomes very weak at low tonic drives. Indeed, $G_{ii}(\psi_{12})$ is almost zero in a neighborhood of $\psi_{12} = \pi$ for $e = 0.05$. This follows from the shape of the PRC, which is almost identically zero over much of its range for small e: see Fig. 4(bottom left).

4 Coupling and phase lags along the cord

As noted in Section 1, two mechanisms have been proposed to account for travelling waves with constant intersegmental phase lags: frequency gradients (Cohen et al. 1982), and asymmetrical coupling strengths (Ermentrout and Kopell 1984). The first permits backward swimming, which lampreys do exhibit in certain circumstances; moreover, increased excitation at the caudal end of the cord has been seen to reverse the sign of phase lags (Matsushima and Grillner 1992). However, lack of consistent frequency gradients in dissected cords, and evidence for asymmetry in ascending/descending coupling (Buchanan 2001; Williams et al. 1990) generally support the second mechanism. We therefore adopt it here.

In spite of extensive experiments, knowledge of intersegmental connectivity remains fragmentary. Because of the apparent lack of segmentation in neural structure other than in ventral and dorsal roots, it is typically assumed that inter- and intrasegmental connections are similar and that the former are local, either via nearest neighbors (Williams 1992), or in case of multiple segments, with strengths that decrease with intersegmental distance. Both schemes produce similar behaviors (Kopell 1990). However, it is also known that there are special interneurons in the CPG having long axonal projections (Buchanan 2001); cf. (Wadden et al. 1997), although little is known about their function.

In this section we assume that intersegmental connections from cell type k in segment j to type l in segment i are of the form $\alpha_{j-i} w_{kl} = \pm\alpha_{j-i}$, implying that *all* coupling strengths between two given segments j and i are equal for arbitrary $j - i$. Strengths α_{j-i} are specified in Section 4.1. Drawing on the theory of Section 2, we may therefore refine the general form of the phase model (1), after averaging, to read

$$\dot{\psi}_i = \sum_{j \in \mathcal{N}(i)} \alpha_{j-i} \bar{H}(\psi_{ij}) \,, \quad i = 1, 2, \ldots, n \,, \tag{14}$$

where ψ_{ij} denotes the phase difference between the ith and jth segments, coupling functions are summed

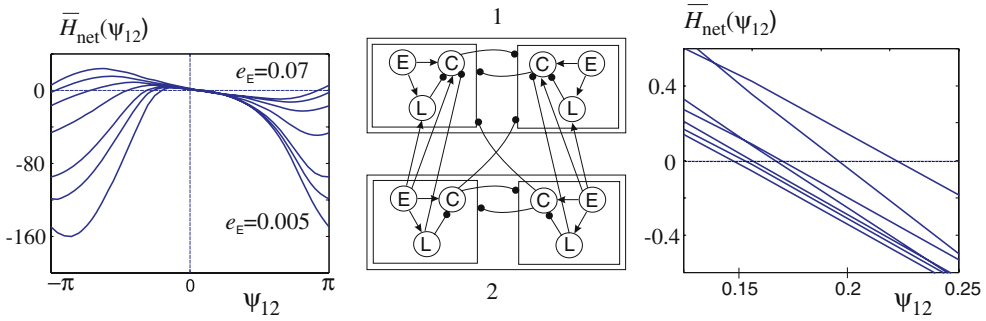

Fig. 6 *Left*: coupling functions for a pair of segments in the network-based model with unidirectional intersegmental coupling and $e_E = 0.005, 0.0075, 0.01, 0.02, 0.04, 0.06, 0.07$, corresponding to a frequency range of $0.015, \ldots, 0.052$. Intrasegmental coupling strengths are equal ($w_{ij} = 1$) as in Section 3.1. *Center*: the segmental network. *Right*: detail of coupling function near $\psi_{12} = 0$

over the connectivity neighborhood $\mathcal{N}(i)$ of the ith segment, and we assume constant frequency along the cord ($\omega_i \equiv \omega_0$).

4.1 The network-based model

In a sufficiently long chain with bi-directional nearest-neighbor intersegmental coupling that is significantly stronger in one direction than in the other, both being much weaker than connections within a segment, intersegmental phase lags between adjacent segments are determined primarily by the dominant direction (Kopell et al. 1991), and they are equal to that of a pair of oscillators with one-way coupling. (Connections in the weaker direction may nonetheless cause boundary effects.) Fig. 6 shows numerically-evaluated coupling functions $\bar{H}_{net}$ for a pair of unidirectionally coupled units over a range of tonic drives (cf. Williams and Bowtell 1997, Fig. 3, but note that there and in Williams 1992) the sign convention differs from ours. The zeroes near $\psi_{12} = 0$ correspond to stable fixed points, and the resulting phase lags $\psi_{12} = \Delta_{net} > 0$, shown in Fig. 7(left), agree well with simulations of Williams (1992) in which ascending intersegmental coupling was assumed to be 2.5 times stronger than descending, and both were significantly weaker ($\approx 1\%$) than intrasegmental connection strengths. Phase lags remain approximately constant over a threefold frequency range, approximating that seen in fictive swimming, but narrower than that of a live swimmer (Williams 1992). Since both segmental models are dimensionless, the frequency scales in Figs. 6, 7 and 9 and 11 (below) are arbitrary.

The phase lag *vs* frequency relation is not especially robust, and behaviors of ostensibly similar models may therefore differ. Even for the present model, parameter changes can disrupt the approximately constant phase lags, as shown in Fig. 7(right), for which the tonic drives were changed to $e_L = e_E$, $e_C = 5e_E$ and e_E was varied from 0.001 to 0.1, in place of the values given in Section 3.1.

The applicability of phase reduction and averaging is questionable for the lamprey CPG, which exhibits relatively strong coupling. We therefore compare a more realistic version of the model of (Williams 1992) to phase reduction-based predictions. We allow bidirectional intersegmental coupling and assume that its strength α_k decays exponentially with distance k, where

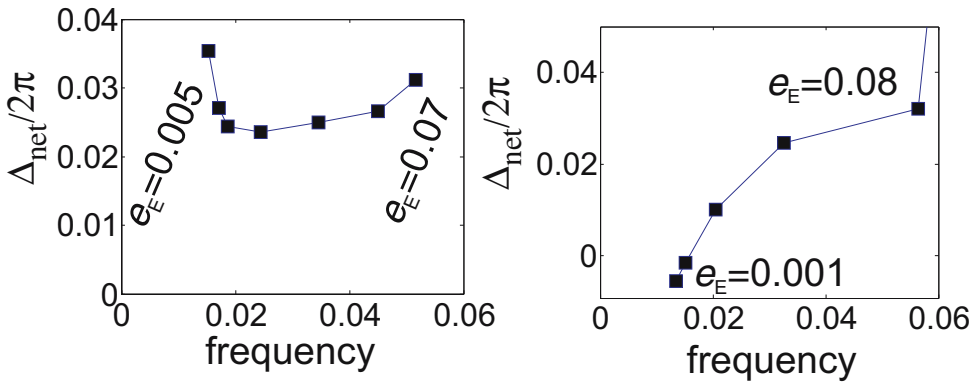

Fig. 7 Average intersegmental phase lags *vs.* oscillator frequency for stable zeroes in the network-based model with weak unidirectional coupling; $\Delta_{net} > 0$ implies that the postsynaptic segment leads. *Left*: tonic drive parameters of Section 3.1. *Right*: modified tonic drives can significantly change phase lags. See text for further discussion

$k > 0$ and $k < 0$ denote ascending and descending connections respectively, see Fig. 8:

$$\alpha_k = \begin{cases} A_d \exp(-|k|/\lambda_d), & \text{if } -l_d \le k \le -1, \\ A_a \exp(-|k|/\lambda_a), & \text{if } 1 \le k \le l_a, \\ 0, & \text{otherwise.} \end{cases} \quad (15)$$

We set $A_d = 0.2$, $A_a = 1$, $\lambda_d = \lambda_a = 1/\ln 2$ and $l_a = l_d = 5$, so that ascending connections are 5 times stronger than descending ones, all strengths decay by a factor of 2 as distance increases by 1, and all connections extend over 5 segments. Various experimental results have been used to argue that ascending coupling is stronger than descending coupling (Williams et al. 1990; Williams and Sigvardt 1994; Kiemel et al. 2003), but the ratio A_a/A_d is not known. Chains of 30 such segments were simulated and the resulting average phase lags are plotted against frequency in Fig. 9. Simulation results for moderate intersegmental strengths are also presented ($A_d = 0.02$, $A_a = 0.1$; other parameters unchanged).

The phase-model-based predictions ignore the weaker descending connections, and the coupling function $\bar{H}_{net}(\psi_{ij})$ is linearised at $\psi_{ij} = \Delta_{net}$, so that $\bar{H}_{net}(\psi_{ij}) \approx \bar{H}'_{net}(\Delta_{net})\,(\psi_{ij} - \Delta_{net})$. From (14) the necessary and sufficient condition for a phase locked solution $\dot{\psi}_i = 0$ with uniform phase lag $\psi_{ij} = \Delta$ per segment is

$$0 = \sum_{j=1}^{5} \alpha_j \bar{H}_{net}(j\Delta) \approx \bar{H}'_{net}(\Delta_{net}) \sum_{j=1}^{5} \alpha_j (j\Delta - \Delta_{net}) , \quad (16)$$

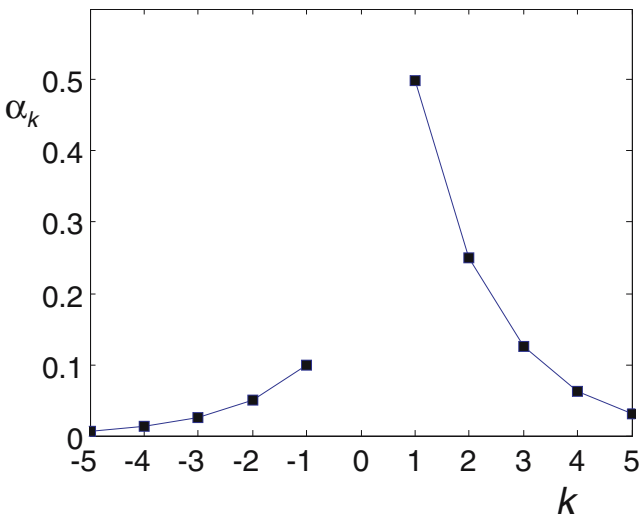

Fig. 8 Intersegmental coupling strengths used in the strong coupling simulations, relative to intrasegmental coupling strength. Abcissa shows connection length in segments, positive for rostrally- and negative for caudally-projecting connections. (Compare with Fig. 14(c) below)

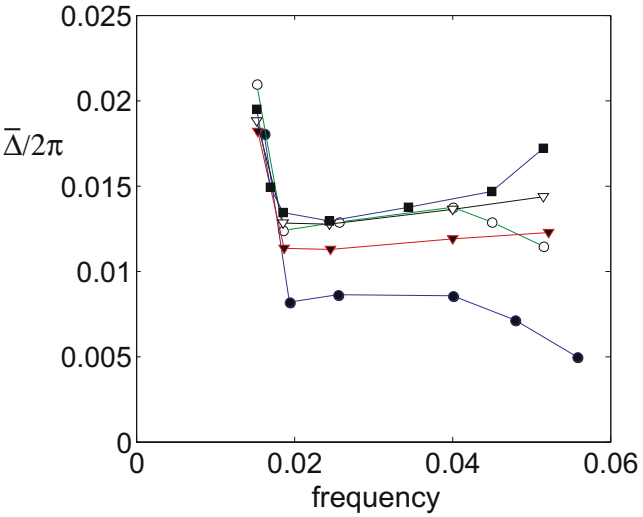

Fig. 9 Average phase lags in the network-based model with bidirectional distributed coupling. *Filled circles*: the strong coupling of Fig. 8. *Open circles*: strong ascending and zero descending coupling. *Filled* and *empty triangles*: coupling with 10% of strong values. *Filled squares*: predictions of phase reduction theory with the coupling strengths of Fig. 8

where $\alpha_j = A_a \exp(-|j|/\lambda_a)$ denotes the strength of length j connections in the dominant (ascending) direction. From (16), and using the strengths shown in Fig. 8, we derive

$$\Delta = \Delta_{net} \frac{\sum_{j=1}^{5} \alpha_j}{\sum_{j=1}^{5} j\alpha_j} \approx 0.54\, \Delta_{net} . \quad (17)$$

This prediction is also shown in Fig. 9, where we see that strong connectivity can modify the weak coupling limit. Specifically, strong ascending and relatively weak descending coupling leads to smaller phase lags (solid circles), but further weakening the descending connections can increase the phase lags (open circles). Nonetheless, the qualitative predictions of phase reduction are preserved and the conclusion that the network-based model can produce near-constant phase lags over a broad frequency range still holds.

4.2 The cell-based model

The cell based model can be analyzed in a similar manner. In Section 3 we showed that contralateral hemisegments oscillate in antiphase. We now consider two segments with one-way coupling. Assuming that ipsi- and contralateral connection strengths are equal ($w_{EE} = 1$, and $w_{EE'} = -1$, respectively), we computed averaged coupling functions (Fig. 10) and their stable zero-crossings (Fig. 11) for a hemisegment that receives excitation from another ipsilateral hemisegment with phase difference ψ_{12}, and inhibition

from a contralateral hemisegment with phase shift $\psi_{12}+\pi$. The function plotted in Fig. 10 is therefore $\bar{H}_{cell}(\psi_{12}) = \bar{H}_e(\psi_{12}) - \bar{H}_e(\psi_{12}+\pi)$, where $\bar{H}_e$ is the excitatory coupling function of Fig. 5(left). Intrasegmental cross-inhibition was not included because this connection uniformly affects every hemisegment in the chain, and therefore does not influence interphase relations.

The most striking result is that the phase lag $\Delta_{cell} < 0$, corresponding to a *phase lead* of the segment that sends the coupling. This suggests that to obtain rostrocaudal phase lags in a cell-based chain, *descending connections must be stronger than ascending ones*, in contrast to the claims of (Williams et al. 1990; Williams and Sigvardt 1994; Kiemel et al. 2003), and to the condition for the network-based model. We were unable to obtain $\Delta_{cell} > 0$ by parameter tuning, but have no explanation for this finding. This does not necessarily imply that the cell-based model is incorrect; indeed, other studies find that descending connections may be stronger (Hagevik and McClellan 1994; McClellan and Hagevik 1999), although they use larval lampreys, and all the experimental studies make modeling assumptions. It is perhaps best to think of the network- and cell-based models as extreme cases in a continuum of CPG architectures. In this sense neither model would be expected to be entirely correct.

However, Fig. 11 shows that phase differences vary significantly with frequency, and parameter tuning did not affect this either. In similar but more detailed models (Wadden et al. 1997; Kotaleski et al. 1999a, b), phase differences were also found to increase with frequency, even when explicit time delays (e.g. synaptic delays) were excluded. This undesirable frequency-dependence of phase seems to be robust in CPGs built of cell-based segmental oscillators, and it is partially understood. Specifically, as noted in Section 3.2, the dominant effect of tonic drive in such models is to change the time constant of the slow AHP dynamics.

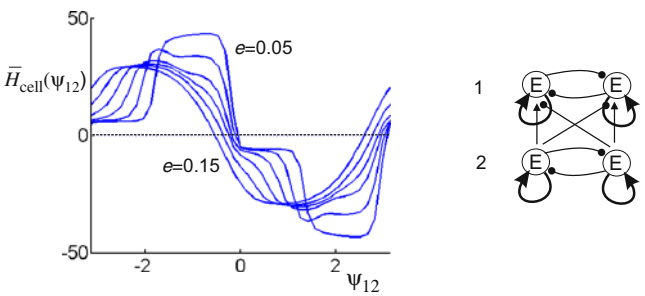

Fig. 10 Coupling functions $\bar{H}_{cell}(\psi_{12})$ for a pair of cell-based segmental oscillators with unidirectional coupling and tonic drives $e = 0.05, 0.07, 0.09, 0.11, 0.13, 0.15$

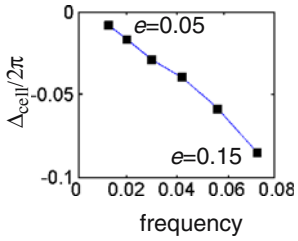

Fig. 11 Phase lags of stable solutions of the cell-based oscillator with unidirectional coupling. In contrast with the network-based model, $\Delta_{cell} < 0$ (the presynaptic unit leads) and Δ_{cell} strongly depends on frequency

Equation (12) implies that, as e decreases, $\tau_i(e)$ increases, so that the oscillators approach their relaxation limit with decreasing frequency. Somers and Kopell (1993) showed that chains of relaxation oscillators with equal ascending and descending coupling rapidly and robustly synchronize. Moreover, chains with asymmetrical coupling, such as lamprey CPG, often exhibit synchrony in spite of the asymmetry (Somers and Kopell 1995), although travelling waves can also occur. Izhikevich (2000) demonstrated that phase reduction techniques yield similar results.

5 Phase reduction for individual connection types in the network-based model

The studies of deterministic intersegmental coupling described in Section 4 assume homogeneity and uniformity along the cord, and, as emphasized, our phase oscillator based results are guaranteed only in the limit of weak coupling. Nonetheless, we have shown that phase oscillator predictions give a good indication of phase lags for a particular case of strong localized coupling (Fig. 8). Here we further investigate the influence of intersegmental connections among different cell types for the network-based model.

In Section 4 we focused on the constancy of adjacent intersegmental phase differences Δ_{net} and Δ_{cell} with swimming frequency. We now examine variations in the phase lag *along the cord*. Phase models with short connections reproduce the near-constant phase lag observed in fictive swimming, but if connection lengths are comparable to that of the chain, significant variations in phase differences between adjacent segments can appear, as illustrated in Fig. 12. Here the maximal connection length is only 1/6 of the total length; however, axons spanning over half the spinal cord length have been identified in lamprey, suggesting that locally-coupled oscillator models are insufficient to explain the data.

Long connections can disrupt phase relations but they also may preserve them if appropriately chosen. Inspired by known differences in the characteristic lengths of different connection types in the spinal

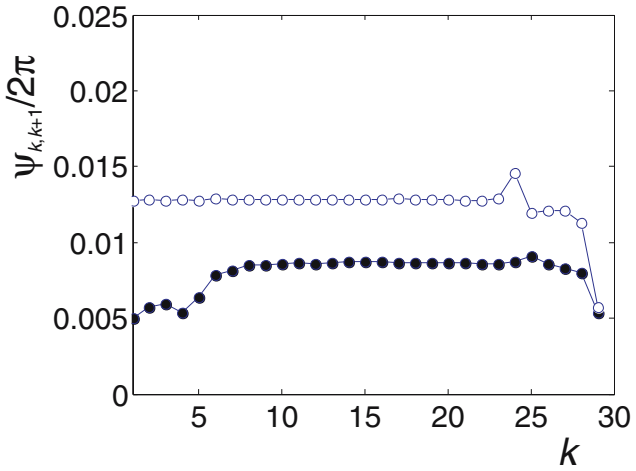

Fig. 12 Phase lags $\psi_{k,k+1}$ between adjacent segments as a function of segment number k for the coupling scheme of Fig. 8, with uni- and bidirectional coupling (*open* and *filled circles* respectively)

cord (Buchanan 2001), we therefore now attempt to tune connection strengths in a manner dependent on their lengths. We use phase reduction to derive separate coupling functions for each connection type. These are then summed to produce the net length-dependent, segment-to-segment coupling. The resulting model allows us to tune coupling with length to produce a uniform traveling wave and, subsequently, to study randomized connections.

5.1 Tuning connections with length

To describe tuning (Mellen et al. 1995), we first consider the phase model

$$\dot{\psi}_i = \sum_{j=1}^{n} \alpha_{j-i} \bar{H}_{j-i}(\psi_{ij}), \qquad i = 1, \ldots, n, \tag{18}$$

which is more general than (14) since both the strength (α) and form ($\bar{H}$) of intersegmental connections may depend on distance ($j-i$). Let $\Delta_{\mathrm{net},k}$ be a stable zero of $\bar{H}_k$ ($\bar{H}_k(\Delta_{\mathrm{net},k}) = 0$ and $\bar{H}_k'(\Delta_{\mathrm{net},k}) < 0$). To tune (18), we choose the $\bar{H}_k$ so that $\Delta_{\mathrm{net},k} = k\Delta$, where Δ is the desired phase lag per segment. The tuned model then has a uniform traveling wave: $\psi_{ij} = (j-i)\Delta$ and the coupling strengths α_k can be varied without affecting phase lags (although stability types may change).

To tune the phase reduction of the network-based neural model (7–8), we choose the $\bar{H}_k$ to have the form

$$\bar{H}_k(\psi) = \sum_{c \in S} w_{k,c} \bar{H}_c(\psi), \tag{19}$$

where $w_{k,c} \geq 0$ are weights, $S = \{EL, EC, LC, CE, CL, CC\}$ is the set of connection types, and $\bar{H}_c$ is the coupling function for connection type c.

The averaged coupling functions $\bar{H}_c$ for default model parameters are shown in Fig. 13. PRCs leading to these functions were computed numerically using the direct method (Hoppensteadt and Izhikevich 1997). Curiously, all six individual functions are rather degenerate, being almost tangent to the horizontal axis near $\psi = 0$. (This is not necessarily true for other parameter values.) The $\bar{H}_{\mathrm{EL}}$, $\bar{H}_{\mathrm{LC}}$ and $\bar{H}_{\mathrm{CC}}$ coupling functions are positive, indicating that these three connection types always speed up the postsynaptic oscillator. In contrast, the $\bar{H}_{\mathrm{EC}}$ and $\bar{H}_{\mathrm{CL}}$ coupling functions are negative, indicating that these two connection types slow down the postsynaptic oscillator. The $\bar{H}_{\mathrm{CE}}$ coupling function has zeros, but primarily slows down the postsynaptic oscillator.

For consistency with Section 4.1, we normalize by setting $\sum_c w_{k,c} = 6$ for all lengths k. In particular, the coupling function $\bar{H}_{\mathrm{net}}$ of Fig. 6 is a special case of $\bar{H}_k$ in which all connection strengths are weighted equally ($w_{k,c} \equiv 1$). Here we denote this coupling function as $\bar{H}(\psi) = \sum_c \bar{H}_c(\psi)$. Another special case of $\bar{H}_k$ results from weighting only connection type c: $\bar{H}_k = 6\bar{H}_c$. Figure 14(a) shows the summed coupling functions $\bar{H}$, $6\bar{H}_{\mathrm{CE}}$ and $6\bar{H}_{\mathrm{EL}}$. $\bar{H}(\psi)$ has a stable zero at $\psi = 0.024$ (cf. Fig. 7, (left)), which moves rightward as $w_{k,\mathrm{EL}}$ increases (thin solid lines in Fig. 14(a) between $\bar{H}$ and $6\bar{H}_{\mathrm{EL}}$). Similarly, increasing $w_{k,\mathrm{CE}}$ moves it leftward. In this way, we can adjust $\bar{H}_k$ to have stable zeros in an interval between the zero of $\bar{H}_{\mathrm{CE}}$ and the near-tangency of $\bar{H}_{\mathrm{EL}}$. Such combined couplings replace the structurally unstable zero crossings of Fig. 13 with a nondegenerate zero.

To determine the potential range of these stable zeros, for each Δ_{net} we adjust the weights $w_{k,c}$ to minimize $\bar{H}_k'(\Delta_{\mathrm{net}})$ subject to the constraint $\bar{H}_k(\Delta_{\mathrm{net}}) = 0$. If the minimum is negative, then Δ_{net} is a potential stable zero and the magnitude $|\bar{H}_k'(\Delta_{\mathrm{net}})|$ indicates the functional strength of $\bar{H}_k$. Adjusting the weights of all connection types, we find that a wide range of Δ_{net} values are potential stable zeros (Fig. 14(b), thin black line), although functional strength is low for some of them. Restricting to the types of $\bar{H}_k$ shown in Fig. 14(a), only values of Δ_{net} from -0.12 to 0.18 are possible: see Fig. 14(b), thick black and grey lines.

We now consider a particular example of a tuned model, restricting our study to the types of $\bar{H}_k$ shown in Fig. 14(a), for simplicity. We adjust the weights $w_{k,c}$ so that the $\bar{H}_k$ are tuned with $\Delta/2\pi = 0.01$ for $-l_d \leq k \leq l_a$, where l_d and l_a are the maximum lengths of descending (caudally-projecting) and ascend-

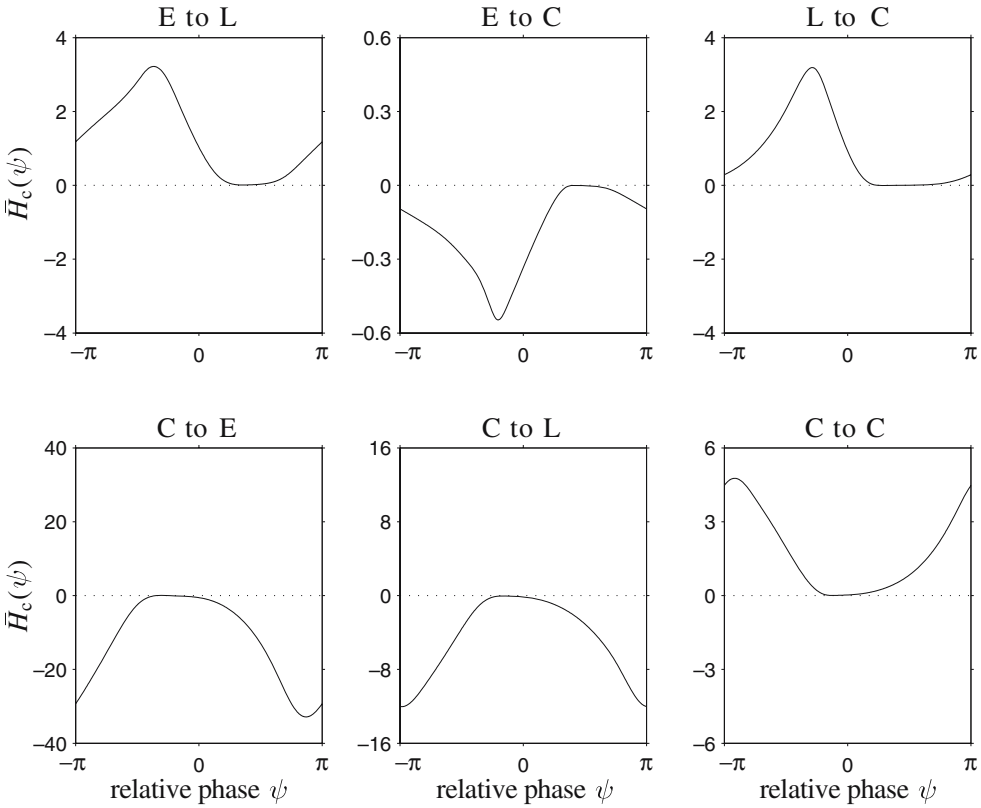

Fig. 13 Coupling functions for each type of connection defined in Section 5.1. Note differences in vertical scales. Tonic drive $e_E = 0.025$

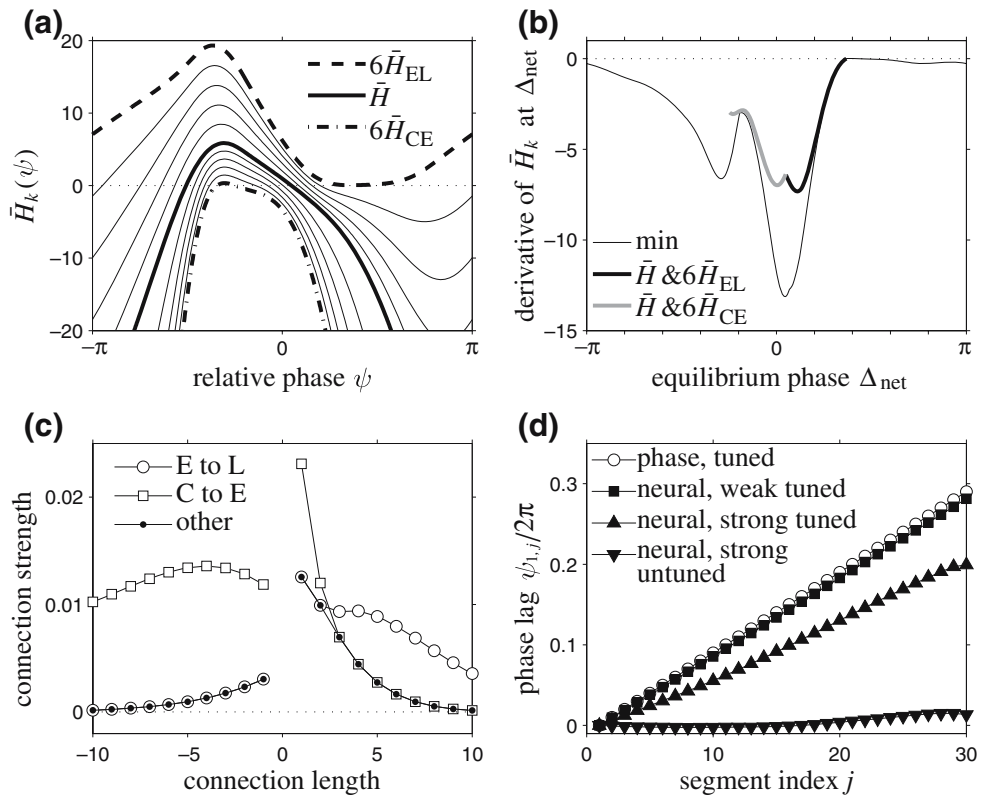

Fig. 14 Tuning the connections. (**a**) Weighted averages $\bar{H}_k$ of coupling functions $\bar{H}$ and $6\bar{H}_{EL}$ and of $\bar{H}$ and $6\bar{H}_{CE}$. (**b**) The derivatives $\bar{H}'_k(\Delta_{net})$. *Thick curves* show the one-parameter family of coupling functions of (**a**); *thin curve* shows minima of the derivative when all weights of Eq. (19) are varied. (**c**) Specified strengths of each connection type as functions of length for a weak coupling example with $A_a = 0.02$, $A_d = 0.005$, $l_a = l_d = 10$, $\lambda_a = 3$, $\lambda_d = 10$. (**d**) Phase lags of travelling wave for tuned phase and neural models with the weak coupling of C and strong coupling with $A_a = 0.4$ and $A_d = 0.1$

ing (rostrally-projecting) connections, respectively, cf. Eq. (15).

The strength $\alpha_{k,c}$ of a connection of length k and type c is given by $\alpha_{k,c} = \alpha_k w_{k,c}$, as shown in Fig. 14(c) for an example with weak coupling. For ascending connections of length $|k| > 2$, $\alpha_{k,c}$ is largest for connections from E to L and is equal for all other types. For ascending connections of lengths 1 and 2 and all descending connections, $\alpha_{k,c}$ is greatest for connection type C to E and is equal for all other types.

Figure 14(d) (open circles) shows the resulting equilibrium phase lags for the phase model with the connection strengths of Fig. 14(c). By construction, the phase lags are exactly 1% per segment. Using the same tuned connection strengths, the neural model with weak coupling (filled squares) closely matches the phase model. Increasing all strengths by a factor of 20 causes a substantial reduction in phase lags of the neural model (filled upward triangles). (Lags predicted by the phase model do not change with strength.) However, even for this level of coupling strength, the model exhibits an approximately uniform traveling wave. In contrast, the neural model with strong untuned connections ($\bar{H}_k \equiv \bar{H}$) fails to exhibit a traveling wave and instead has intersegmental phase lags near zero (filled downward triangles). The phase lags for this untuned model are smaller than for the untuned models shown of Fig. 9, because the present example has longer connections (compare Figs. 8 and 14(c)). The wider the range of connection lengths, the greater the effect that tuning has on phase lags.

As previously noted in Section 4.1, the robustness of phase lags in the network-based model to frequency changes does not necessarily persist when model parameters are changed. Just as modifying tonic drives can reduce robustness (Fig. 7), so can tuning of connections. However, the presence of long connections can at least partially restore robust phase lags, as illustrated in Fig. 15. When tuned connection strengths decay rapidly with distance (small λ_d and λ_a), phase lags show strong dependence on frequency, but as longer connections become more prominent (increasing λ_d and λ_a), frequency dependence weakens. This suggests that adding longer connections might be a general mechanism to make phase lags more uniform over a wide frequency range (see Section 6).

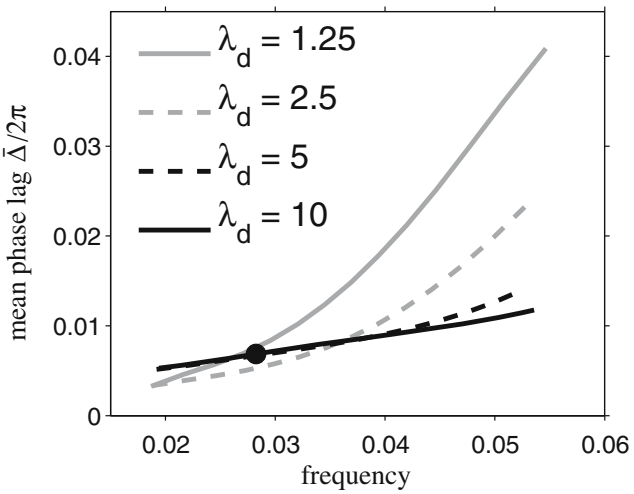

Fig. 15 Effect of connection lengths on robustness of phase lags. Mean phase lag between adjacent oscillators is plotted as a function of frequency. Changes in frequency are produced by varying the tonic drive e_E from 0.010 (low frequency) to 0.075 (high frequency) for four different values of λ_d describing the decay of coupling strength with length. In each case, $A_a = 0.4$, $A_d = 0.1$, $l_a = l_d = 10$, $\lambda_a = 0.3\lambda_d$, and connections were tuned with $\Delta/2\pi = 0.01$ based on the coupling functions for $e_E = 0.025$ (Fig. 13). *Filled circle* corresponds to the strong tuned neural model of Fig. 14(d)

5.2 A chain with random connections

In common with all complex organisms, lampreys exhibit considerable individual variety with respect to connectivity. To address this, we now modify the examples of Section 5.1, replacing the prescribed deterministic connections by random intersegmental connections. Although *intra*-segmental connections could also be chosen randomly, for simplicity we only randomize the intersegmental connections.

In contrast to the deterministic coupling of Section 5.1, all connections in the random model are given equal strength, but some are assigned a higher probability of being chosen more than once, thus effectively producing a range of strengths between each pair of segments. Each connection is chosen randomly based on a Poisson distribution, with probability proportional to connection lengths and strengths in the tuned deterministic model (see Fig. 14(c)). Stronger connections in the deterministic model thus induce higher probabilities of choosing those connections in the random model. In this way, different connection strengths are reflected in the number of times that a given connection from i to j is chosen. Since the strength of each connection is inversely proportional to the mean of the distribution, as the number of connections becomes large, the random model approaches the deterministic model.

As in Fig. 14(d), Fig. 16 illustrates the phase lag relative to the first segment, but for random connections. Two particular simulations are shown in Fig. 16 for both the randomly-connected neural and the phase models, with weak coupling above and strong coupling below. In both panels the average number of connections is 200. Dotted and dashed lines show the phases of the

deterministic phase and neural models respectively. Squares and circles denote results from two different simulations (see key on panels).

In contrast, Fig. 17 illustrates convergence of the random models to the deterministic models in terms of mean phase lag, as the average number of connections per segment grows. The mean phase lag per segment is computed by first finding the mean phase lag over the thirty oscillators, then computing the mean and standard deviation over the fifty simulations. It also corresponds to the slope of linear fits to the data in Fig. 16. Figure 17 shows that both the strongly and weakly coupled neural models, indicated by triangles and squares, converge to the mean phase of the deterministic neural models, indicated by the dotted lines.

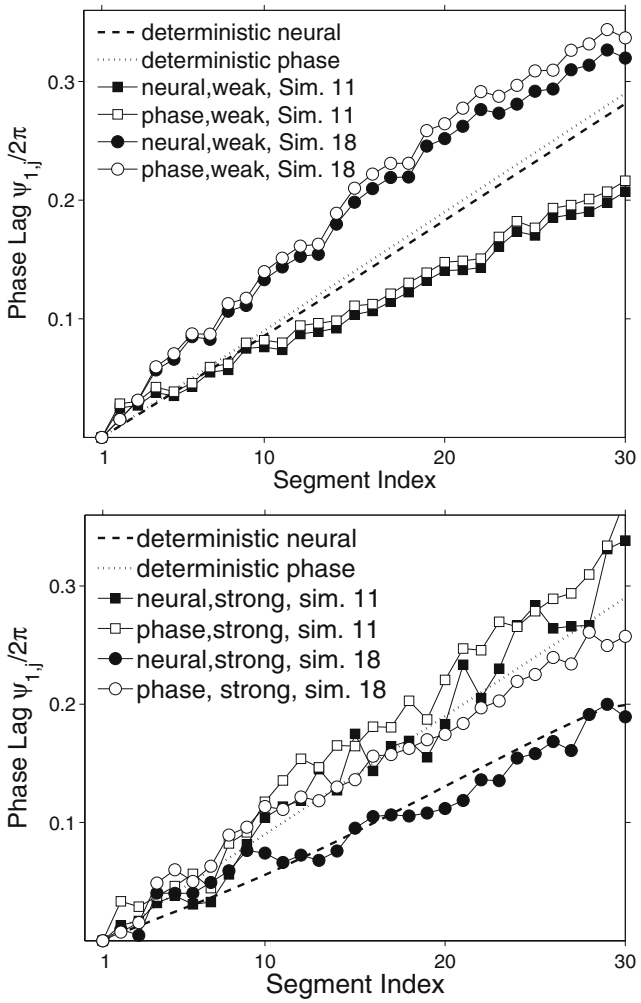

Fig. 16 Phase lags for the randomly-coupled model. Each panel shows two examples of the phase lag relative to the first segment plotted as a function of segment number for weak (*top*) and strong (*bottom*) connections. The *dotted line* is the phase lag with respect to the first oscillator for the deterministic phase model and the *dashed line* is the mean phase lag for the tuned deterministic neural model. The average number of connections for these examples is 200

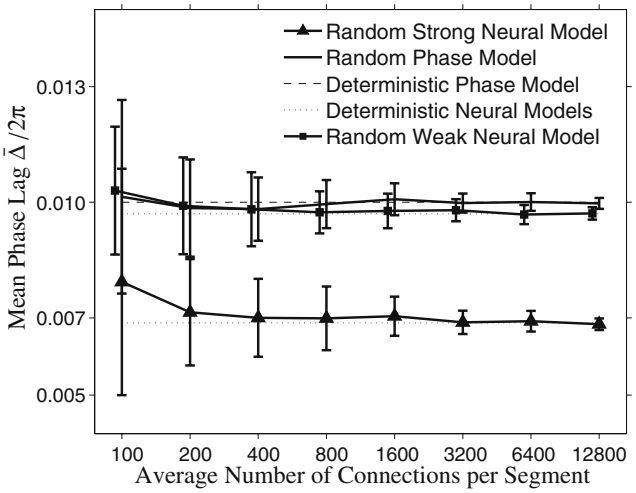

Fig. 17 Mean and standard deviation of the phase lag per segment are shown for increasing mean number of connections for both the neural model with strong and weak connections and the phase model (data are identical for strong and weak connections, so only one line is shown), as indicated in the legend. Note that the mean phase lag of models with randomly generated connections approaches the mean phase lag per segment of the deterministic models, as the average number of connections gets larger

The random phase model is represented by the solid line that converges to the mean phase of the deterministic phase model, shown by the dashed line. Standard deviations (error bars) decrease as the average number of connections per segment increases. An average of 100 connections per segment seems to be the point at which the oscillators are almost certainly phase locked. Below 100, the chances of the oscillators not achieving phase locking increases significantly. This figure is consistent with typical cell and axonal densities in lamprey spinal cord. Although there is no direct experimental evidence regarding the number of connections per segment, with about 1000 neurons per segment, it is reasonable to expect at least 100 connections per segment.

6 Summary and discussion

In this paper we have used phase response and averaging theory (Sections 2–3) to compute intersegmental coupling functions for network- and cell-based models of lamprey central pattern generators (Section 4). We find that, while the coupling functions thus derived are qualitatively similar to the sinusoids assumed in early phase models, they differ sufficiently from them and from each other that their traveling wave solutions, characteristic of fictive swimming *in vitro*, behave in qualitatively distinct manners as swimming frequency

varies. In particular, while ascending and descending couplings in the network-based model can be tuned in a biologically-reasonable manner to produce a near-constant phase lag of $\approx 1\%$ per segment over the appropriate frequency range (Fig. 7(left)), the cell-based model is less robust in that its phase lags tend to decrease with frequency, and can even change sign as frequency increases (Fig. 11).

The results of Section 4 also show that phase models, derived under the assumption of weak coupling, can nonetheless give results indicative of traveling wave behavior for oscillator chains with coupling strengths more realistic for lamprey. In Section 5 we exploit this, using phase response theory to probe the contributions of connections among specific cell types in the network-based model, to intersegmental coupling and to phase lags in the resulting traveling waves. We find that, while individual coupling functions tend toward structural instability (Guckenheimer and Holmes 1983) (Fig. 13), linear superpositions of them can be tuned to produce stable traveling waves over a reasonable frequency range (Fig. 14), and moreover that random connections drawn from probability distributions of strengths and lengths characteristic of lamprey data also produce robust traveling waves (Fig. 16).

We end by discussing two aspects of this work of particular relevance to modeling CPGs of lamprey CPG and of anguilliform swimmers in general.

6.1 Robustness of constant phase lag vs. frequency

We propose three possible mechanisms to explain the fact that approximately-constant $\approx 1\%$ per segment lags are observed over the animal's range of swimming speeds, but that phase lags can be disrupted by perturbations in coupling strength, even for the network-based model (Fig 7(right)).

1. *Descending input from the brainstem preserves phase lags as frequency changes* The necessary constraint in the network-based model of (Buchanan 1992; Williams 1992) is that tonic drives to the crossed inhibitory (C) and lateral interneurons (L) should remain constant as the drive e_E to the excitatory interneurons (E) is varied. However, this particular constraint is due to the specific parameterization in (Williams 1992) that was also adopted here (Section 3.1). In general, given a parameterization of the CPG model, all three tonic drives would have to be changed in a coordinated way to preserve the desired phase lags. There is also the possibility that changes in tonic drives vary systematically along the length of the spinal cord (not examined here).
2. *Due to long distance connections, phase lags depend only weakly on spinal cord activation* In general, as longer connections become more prominent, phase lags become less sensitive to changes in activation (Fig. 15). This mechanism does not require a specific activation pattern, consistent with the fact that activation of the spinal cord by bath application of drugs *in vitro* with brain and brainstem removed produces phase lags that approximate those seen in swimming *in vivo*. A special case would be to have 50-segment-long connections impose phase differences of π (Cohen et al. 1982; Ermentrout and Kopell 1994a). However, although such long "anti-phase" connections can potentially produce very robust lags, they are not thought to be the primary mechanism for phase regulation in the lamprey CPG, since pieces of spinal cord as short as 20 segments exhibit phase lags characteristic of intact animals (Williams and Sigvardt 1994).
3. *Phase lags are tuned by a self-regulating mechanism* Ermentrout and Kopell (1994b) studied a CPG network model in which phase lags are led toward constancy by a higher-order "teaching" network. Such mechanisms have not been identified in lamprey, but neural plasticity can facilitate network regulation, and it is present in the lamprey although its role is unclear (Parker 2006). Identification of a self-regulating effect could resolve the conflict between the robustness of the biological network and the sensitivity of current computational models.

In the intact animal, proprioceptive neural feedback (e.g., from edge cells) and mechanical connectivity afforded by muscles and body tissues may provide substantial additional constraints and help establish and stabilize traveling waves. However, *in vitro* studies with muscles and sensory inputs removed show that these components are not necessary.

6.2 Does intersegmental coupling vary systematically with length?

In Section 5.1 we showed how a phase model can be used to tune coupling in a neural model so that it exhibits an approximately uniform traveling wave. Tuning involves varying the relative strengths of different connection types systematically with length. Such variations do exist in the lamprey CPG. For example, only lateral interneurons are known to project to distances as long as 50 segments (Rovainen 1974), so the relative strength of L to C connections compared to

other connection types would be expected to increase with distance. What is not known is whether the variation of relative strength with length in the lamprey CPG follows the pattern of tuning. For example, if connections are tuned and only L to C connections exist at length 50, then this connection type should have a stable relative phase of around π, since phase lags are about 1% per segment. This is not true for the network-based model with our default parameters (Fig. 13). However, it may be a limitation of the model, which was originally developed with only nearest-neighbor connections (Williams et al. 1990; Williams and Bowtell 1997).

From Fig. 14(b), we see that the model is most effective in stabilizing phases of less than 0.2. However, connections of lengths greater than 20 provide substantial coupling (Rovainen 1985; Miller and Sigvardt 2000; Kiemel et al. 2003). This suggests that the model should be modified to increase the effectiveness of long connections. The two options are to change model parameters or to fundamentally change the structure of the model. In terms of the second option, it may be useful to explore the idea that the cell types that mediate long distance coupling, such as laternal interneurons, are not required to produce oscillation (Parker 2006).

Laternal interneurons are essential for oscillation in the network-based model, since they provide the only inhibition within a hemisegment. Introducing additional cell types or cellular properties to assume the oscillatory role of the LINs and/or combining the network-effect with cell-based oscillators may provide sufficient freedom to develop a model in which these cells are able to provide effective long distance coupling.

Acknowledgements This work was supported by NSF EF-0425878 and NIH NS054271. PV was supported by Imre Korányi and Zoltán Magyary fellowships as well as by OTKA-72368, and hosted by the Program in Applied and Computational Mathematics of Princeton University. KH was supported by NSF DMS-0624024, and hosted by the Department of Biology, University of Maryland College Park. KH also gratefully acknowledges the computing resources of the Department of Mathematics and Statistics at University of Maryland Baltimore County.

References

Buchanan, J. T. (1982). Identification of interneurons with contralateral, caudal axons in the lamprey spinal cord: Synaptic interactions and morphology. *Journal of Neurophysiology, 47*, 961–975.

Buchanan, J. T. (1992). Neural network simulations of coupled locomotor oscillators in the lamprey spinal cord. *Biological Cybernetics, 66*, 367–374.

Buchanan, J. T. (1999). Commissural interneurons in rhythm generation and intersegmental coupling in the lamprey spinal cord. *Journal of Neurophysiology, 81*, 2037–2045.

Buchanan, J. T. (2001). Contributions of identifiable neurons and neuron classes to lamprey vertebrate neurobiology. *Progress in Neurobiology, 63*, 441–466.

Buchanan, J. T., & Grillner, S. (1987). Newly identified glutamate interneurons and their role in locomotion in the lamprey spinal cord. *Science, 236*, 312–314.

Cangiano, L., & Grillner, S. (2003). Fast and slow locomotor burst generation in the hemispinal cord of the lamprey. *Journal of Neurophysiology, 89*, 2931–2942.

Cohen, A. H., Ermentrout, G. B., Kiemel, T., Kopell, N., Sigvardt, K. A., & Williams, T. L. (1992). Modelling of intersegmental coordination in the lamprey central pattern generator for locomotion. *Trends in Neuroscience, 15*, 434–438.

Cohen, A. H., Holmes, P. J., & Rand, R. H. (1982). The nature of the coupling between segmental oscillators of the lamprey spinal generator for locomotion: A mathematical model. *Journal of Mathematical Biology, 13*, 345–369.

Cohen, A. H., Rossignol, S., & Grillner, S. (Eds.) (1988). *Neural control of rhythmic movements in vertebrates*. New York: Wiley.

Cohen, A. H., & Wallén, P. (1980). The neuronal correlate of locomotion in fish. 'Fictive swimming' induced in an *in vitro* preparation of the lamprey. *Experimental Brain Research, 41*, 11–18.

Ekeberg, O. (1993). A combined neuronal and mechanical model of fish swimming. *Biological Cybernetics, 69*, 363–374.

Ermentrout, G. B. (1996). Type I membranes, phase resetting curves, and synchrony. *Neural Computation, 8*, 979–1001.

Ermentrout, G. B., & Kopell, N. (1984). Frequency plateaus in a chain of coupled oscillators. *SIAM Journal on Mathematical Analysis, 15*, 215–237.

Ermentrout, G. B., & Kopell, N. (1991). Multiple pulse interactions and averaging in systems of coupled neural oscillators. *Journal of Mathematical Biology, 29*, 195–217.

Ermentrout, G. B., & Kopell, N. (1994a). Inhibition-produced patterning in chains of coupled nonlinear oscillators. *SIAM Journal on Applied Mathematics, 54*, 478–507.

Ermentrout, G. B., & Kopell, N. (1994b). Learning of phase lags in coupled neural oscillators. *Neural Computation, 6*, 225–241.

Getting, P. A. (1988). Comparative analysis of invertebrate central pattern generators. In A. H. Cohen, S. Rossignol, & S. Grillner (Eds.), *Neural control of rhythmic movements in vertebrates* (chapter 4, pp. 101–128). New York, NY: John Wiley.

Ghigliazza, R. M., & Holmes, P. (2004a). A minimal model of a central pattern generator and motoneurons for insect locomotion. *SIAM Journal on Applied Dynamical Systems, 3*(4), 671–700.

Ghigliazza, R. M., & Holmes, P. (2004b). Minimal models of bursting neurons: How multiple currents, conductances and timescales affect bifurcation diagrams. *SIAM Journal on Applied Dynamical Systems, 3*(4), 636–670.

Grillner, S. (2003). The motor infrastructure: From ion channels to neuronal networks. *Nature Reviews Neuroscience, 4*, 573–586.

Grillner, S., Buchanan, J. T., & Lansner, A. (1988). Simulation of the segmental burst generating network for locomotion in lamprey. *Neuroscience Letters, 89*, 31–35.

Guckenheimer, J., & Holmes, P. J. (1983). *Nonlinear oscillations, dynamical systems and bifurcations of vector fields*. New York: Springer.

Hagevik, A., & McClellan, A. D. (1994). Coupling of spinal locomotor networks in larval lamprey revealed by receptor blockers for inhibitory amino acids: Neurophysiology and computer modeling. *Journal of Neurophysiology, 72*, 1810–1829.

Harris-Warrick, R. M., & Cohen, A. H. (1985). Serotonin modulates the central pattern generator for locomotion in the isolated lamprey spinal-cord. *Journal of Experimental Biology, 116*, 27–46.

Hellgren, J., Grillner, S., & Lansner, A. (1992). Computer simulation of the segmental neural network generating locomotion in lamprey by using populations of network interneurons. *Biological Cybernetics, 68*, 1–13.

Hoppensteadt, F. C., & Izhikevich, E. M. (1997). *Weakly connected neural networks*. New York: Springer.

Izhikevich, E. M. (2000). Phase equations for relaxation oscillators. *SIAM Journal on Applied Mathematics, 60*, 1789–1804.

Kiehn, O. (2006). Locomotor circuits in the mammalian spinal cord. *Annual Review of Neuroscience, 29*, 279–306.

Kiemel, T., Gormley, K. M., Guan, L., Williams, T. L., & Cohen, A. H. (2003). Estimating the strength and direction of functional coupling in the lamprey spinal cord. *Journal of Computational Neuroscience, 15*, 233–245.

Kopell, N., & Ermentrout, G. B. (1988). Coupled oscillators and the design of central pattern generators. *Mathematical Biosciences, 90*, 87–109.

Kopell, N., Ermentrout, G. B., & Williams T. L. (1991). On chains of oscillators forced at one end. *SIAM Journal on Applied Mathematics, 51*, 1397–1417.

Kopell, N., Zhang, W., & Ermentrout, G. B. (1990). Multiple coupling in chains of oscillators. *SIAM Journal on Mathematical Analysis, 21*, 935–953.

Kotaleski, J. H., Grillner, S., & Lansner, A. (1999a). Neural mechanisms potentially contributing to the intersegmental phase lag in lamprey I. Segmental oscillations dependent on reciprocal inhibition. *Biological Cybernetics, 81*, 317–330.

Kotaleski, J. H., Lansner, A., & Grillner, S. (1999b). Neural mechanisms potentially contributing to the intersegmental phase lag in lamprey II. Hemisegmental oscillations produced by mutually coupled excitatory neurons. *Biological Cybernetics, 81*, 299–315.

Kristan, W. B., Calabrese, R. L., & Friesen, W. O (2005). Neuronal control of leech behavior. *Progress in Neurobiology, 76*, 279–327.

Kuramoto, Y. (1984). *Chemical oscillations, waves, and turbulence*. Berlin: Springer.

Lansner, A., Ekeberg, O., & Grillner, S. (1997). Realistic modeling of burst generation and swimming in the lamprey. In P. S. G. Stein, S. Grillner, A. I. Selverston, & D. G. Stuart (Eds.), *Neurons, networks and motor behavior*. Cambridge, MA: MIT Press.

Malkin, I. G. (1949). *Methods of Poincaré and Linstedt in the theory of nonlinear oscillations*. Moscow: Gostexisdat (in Russian).

Malkin, I. G. (1956). *Some problems in nonlinear oscillation theory*. Gostexisdat: Moscow (in Russian).

Matsushima, T., & Grillner, S. (1992). Neural mechanisms of intersegmental coordination in lamprey: Local excitability changes modify the phase coupling along the spinal cord. *Journal of Neurophysiology, 67*, 373–388.

McClellan, A. D., & Hagevik, A. (1999). Coordination of spinal locomotor activity in the lamprey: Long-distance coupling of spinal oscillators. *Experimental Brain Research, 126*, 93–108.

Mellen, N., Kiemel, T., & Cohen, A. H. (1995). Correlational analysis of fictive swimming in the lamprey reveals strong functional intersegmental coupling. *Journal of Neurophysiology, 73*(3), 1020–1030.

Miller, W. L., & Sigvardt, K. A. (2000). Extent and role of multisegmental coupling in the lamprey spinal locomotor pattern generator. *Journal of Neurophysiology, 83*, 465–476.

Parker, D. (2006). Complexities and uncertainties of neural network function. *Philosophical Transactions of the Royal Society of London B, 361*, 81–99.

Pearson, K. G. (2000). Motor systems. *Current Opinion in Neurobiology, 10*, 649–654.

Rovainen, C. M. (1974). Synaptic interactions of identified nerve cells in the spinal cord of the sea lamprey. *Journal of Comparative Neurology, 154*, 189–206.

Rovainen, C. M. (1985). Effects of groups of propriospinal interneurons on fictive swimming in the isolated spinal cord of the lamprey. *Journal of Neurophysiology, 54*, 959–977.

Schotland, J. L., & Grillner, S. (1993). Effects of serotonin on fictive locomotion coordinated by a neural network deprived of NMDA receptor-mediated cellular properties. *Experimental Brain Research, 93*, 391–398.

Somers, D., & Kopell, N. (1993). Rapid synchronization through fast threshold modulation. *Biological Cybernetics, 68*, 393–407.

Somers, D., & Kopell, N. (1995). Waves and synchrony in networks of oscillators of relaxation and non-relaxation type. *Physica D, 89*, 169–183.

Wadden, T., Hellgren, J., Lansner, A., & Grillner, S. (1997). Intersegmental coordination in the lamprey: Simulations using a network model without segmental boundaries. *Biological Cybernetics, 76*, 1–9.

Wallen, P., Ekeberg, O., Lansner, A., Brodin, L., Traven, H., & Grillner, S. (1992). A computer-based model for realistic simulations of neural networks. II. The segmental network generating locomotor rhythmicity in the lamprey. *Journal of Neurophysiology, 68*, 1939–1950.

Williams, T. L. (1992). Phase coupling by synaptic spread in chains of coupled neuronal oscillators. *Science, 258*, 662–665.

Williams, T. L., & Bowtell, G. (1997). The calculation of frequency-shift functions for chains of coupled oscillators, with application to a network model of the lamprey locomotor pattern generator. *Journal of Computational Neuroscience, 4*, 47–55.

Williams, T. L., & Sigvardt, K. A. (1994). Intersegmental phase lags in the lamprey spinal cord: Experimental confirmation of the existence of a boundary region. *Journal of Computational Neuroscience, 1*, 61–67.

Williams, T. L., Sigvardt, K. A., Kopell, N., Ermentrout, G. B., & Remler, M. P. (1990). Forcing of coupled nonlinear oscillators: Studies of intersegmental coordination in the lamprey locomotor central pattern generator. *Journal of Neurophysiology, 64*, 862–871.

Williams, T. L., & Wallén, P., (1984). Fictive locomotion in the lamprey spinal cord *in vitro* compared with swimming in the intact and spinal animal. *Journal of Physiology, 347*, 225–239.

Wilson, H. (1999). *Spikes, decisions and actions: The dynamical foundations of neuroscience*. Oxford: Oxford University Press.